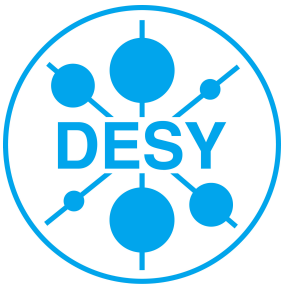

Measurement of the Momentum Spread of a DESY Test-Beam Line Using CMS Pixel Modules

Ricardo Wölker
University of Manchester, Manchester, UK

Supervisors:
Daniel Pitzl Paul Schütze
DESY, Hamburg, Germany

September 7, 2016

Abstract

The DESY test-beam area 21 (TB21) delivers electron beams of energies between 1 and 6 GeV. The momentum spread is claimed to be $\sim 5\%$ with an angular divergence of ~ 1 mrad, which has thus far not been verified experimentally. Measurements of the momentum spread and angular divergence of TB21 using CMS upgrade silicon pixel detectors in a magnetic dipole field are here presented. The relative momentum spread is found to be 2.02 ± 0.01 (stat) $^{+0.92}_{-0.18}$ (sys) % at high momentum ($p = 5.6$ GeV/c), increasing to 12.86 ± 0.02 (stat) $^{+2.78}_{-2.56}$ (sys) % at low momentum ($p = 1.0$ GeV/c). The reconstructed electron momentum is shown to agree with the nominal test-beam momentum within systematic uncertainties. The angular divergence is confirmed to be consistent with the tabulated value at 0.96 ± 0.01 (stat) $^{+0.03}_{-0.04}$ (sys) mrad at $p = 2.8$ GeV/c.

Contents

1 Introduction

DESY II is a 293 m long circular electron synchrotron located at the DESY site in Hamburg. Serving primarily as an injector for the PETRA III accelerator, it also provides electrons of energies of from 1 to 6 GeV for three test-beam lines located in Hall 27 at the DESY site. It is currently claimed [12] that the electrons (and positrons) in the test-beam lines of energies from 1 to 6 GeV have a momentum spread of $\sim 5\%$ and an angular divergence of ~ 1 mrad. It is noted that there have so far not been any experiments to verify these numbers.

This report describes the experimental verification of these figures, undertaken from July to September 2016. The experiment is performed using silicon pixel detectors as to be implemented into the Compact Muon Solenoid (CMS) experiment at CERN's Large Hadron Collider (LHC) as part of the pixel upgrade in 2017 [11]. In particular, it is found that the momentum spread strongly depends on the beam momentum selected, varying from $\sim 2\%$ to $\sim 18\%$, and that the angular divergence approaches ~ 0.6 mrad at high momenta.

2 Background

2.1 CMS Pixel Detector

The CMS experiment at the LHC is a high-energy particle physics detector designed to study proton-proton collisions at a centre-of-mass energy of up to 14 TeV [3]. The innermost part of the experiment consists of three layers of silicon pixel detectors of radii between 4.2 and 10.2 cm. The pixel detectors are located close to the interaction point to provide accurate measurements of charged-particle tracks. Fig. 1 shows the current arrangement of the pixel detectors around the beam pipe.

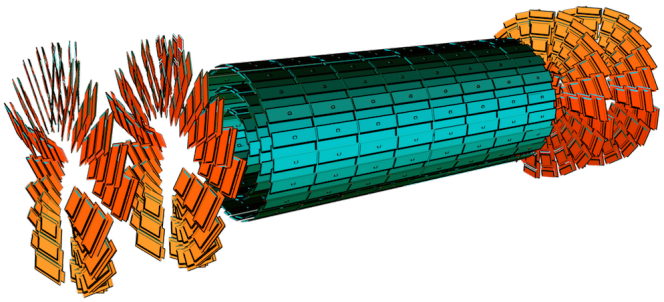

Figure 1: Schematic drawing of the current CMS pixel detector [1]. The pixel modules investigated here are shown in green. They are arranged cylindrically around the beam pipe with radii between 4.2 cm and 10.2 cm. The scale of this unit is ~ 30 cm in diameter and ~ 100 cm in length.

2.1.1 CMS Pixel Modules

In its current configuration, the entire CMS pixel detector setup consists of 1440 so-called *modules*. The data collected by each module are read out by 16 read-out chips (ROCs). Each of these ROCs in turn consists of $80 \times 52 = 4160$ pixels with a size (*pitch*) of 100 μm $\times$150 μm, amounting to a total of 66560 pixels per module. Fig. 2 shows one such module. A complete description of the CMS pixel modules is given in Ref. [7].

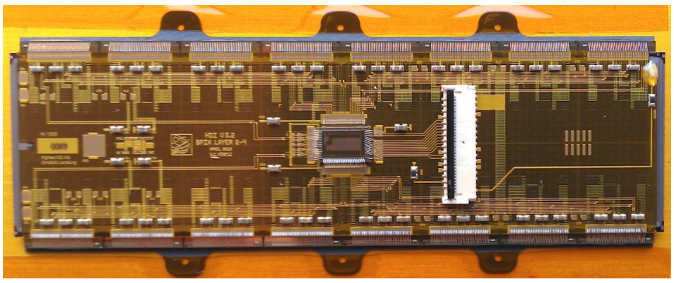

Figure 2: CMS pixel module. Image: D. Pitzl.

2.1.2 Setup

Within the scope of this report, we consider a setup of four modules that are mounted on a rotatable plate and placed inside a homogeneous magnetic dipole field. We place our experiment in a Cartesian coordinate system; let the beam direction be along positive z, the magnetic field along negative y, and let the plate lie within the x-z plane. The modules are labelled A, B, C, and D, and are spaced 103 mm (A-B and C-D), and 32 mm (B-C) apart. Relative to the x-z plane, the modules have a forwards *tilt*, α, of 19°. Additionally, the modules have a *turn*, ω, of 27° relative to the z-axis, when the plate is in a neutral position, i.e. the *rotation* angle, ϕ, equals zero. At $\phi = 0$, both α and ω are chosen such that an incident electron is likely to excite three pixels at once (have a *cluster size* of three). This cluster size is desirable to allow for a more accurate track reconstruction and better resolution, as it makes possible a triangulation of the hit based on the fractional charge deposition in the individual pixels. Fig. 3 shows the set of four modules used in this study.

2.2 DESY Test-Beam Generation

The 293-m DESY II circular synchrotron stores electrons of energies up to 6 GeV. Mainly an injector for the larger PETRA III experiment, it also serves as an electron (positron) source for experiments in the DESY *test-beam* lines.

The stored electrons are incident on a carbon fibre target, which, due to an abrupt deceleration of the electrons, causes them to emit high-energetic photons (bremsstrahlung radiation). The photons are directed at a *converter target* (4 mm of copper), which emits

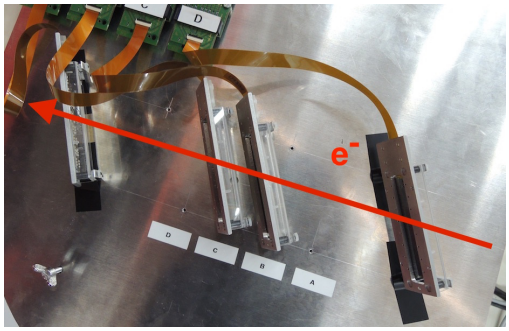

Figure 3: Four CMS pixel modules mounted on a plate, with its axis of rotation mid-way between modules B and C. The incident electron path, in the absence of a magnetic field, is indicated by the red arrow. Image: D. Pitzl.

an electron-positron pair of energies from 0 to 6 GeV upon photon incidence. The particles traverse a spectrometer magnet that selects the desired particle type (e^+ or e^-) and discriminates the particles according to their momentum, at which point only electrons (positrons) of a specific momentum set by the operator are able to pass through. The final stage of beam generation consists of a *collimator* which aims to make the electron beam narrower and more parallel. The process of test-beam generation with DESY II and the test-beam areas are shown in Fig. 4.

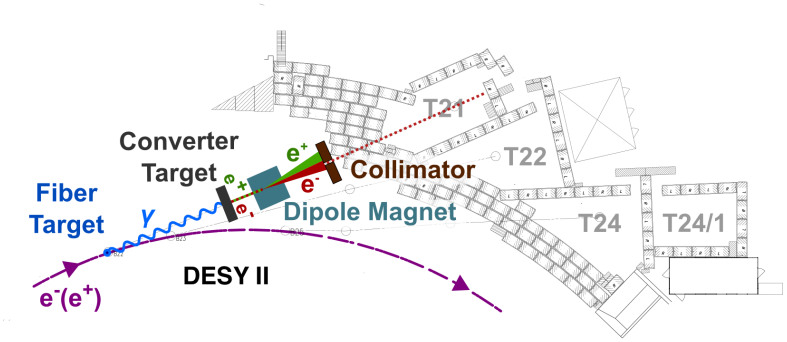

Figure 4: Layout of the DESY II electron synchrotron with the adjacent test-beam lines [12]. Electrons inside the synchrotron hit a fibre target, which emits bremsstrahlung photons. A converter target (Cu or Al) converts the photons into an e^+e^- pair. A subsequent magnet and collimator allow for selection of the particle type and momentum. The measurements presented here were performed in beam area 21, labelled *T21* in this drawing, and referred to as *TB21* in this report.

2.2.1 TB21

Within TB21, one can perform experiments in a magnetic field by making use of a strong dipole magnet which produces a homogeneous field of up to 1.35 T at a coil current of 1400 A [10]. The magnetic field bends the electron trajectory perpendicularly to both the field lines and the electron velocity, causing the electrons to follow a curved path. Measuring the radius, or, equivalently, the curvature, of the path allows for the

reconstruction of the electron momentum, p. The details of the momentum measurement are discussed in Sec. 3. The four modules within the magnetic dipole field are depicted in Fig. 5.

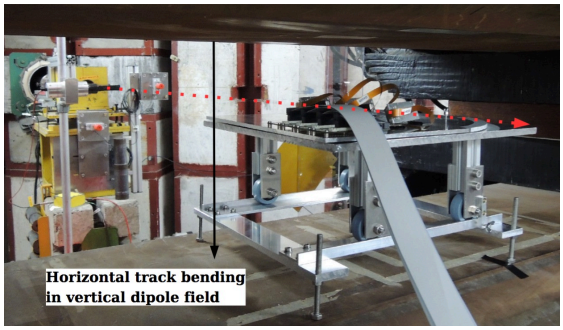

Figure 5: Four CMS silicon pixel modules mounted on a rotatable plate inside the homogeneous field of a dipole magnet. The incident electrons are indicated by the dashed red line, and the direction of the dipole field lines by the black arrow. The electrons are bent in the horizontal plane due to the Lorentz force (Sec. 3.1).

2.3 Multiple Scattering

A charged particle passing through matter is scattered by small angles as it interacts with the atomic nuclei via Coulomb scattering [4]. The central limit theorem predicts that many of these small-angle scatters are normally distributed around zero. If θ_{ms} is a measure proportional to the angular spread of the multiply scattered particles, we have from [4, eq. 32.15], in the highly relativistic limit[a] and up to constant factors

$$\theta_{\text{ms}} = \frac{1}{p} \times f(d), \tag{1}$$

where $f(d)$ is some function of the thickness, d, of the material traversed. We note that the tracking resolution scales with θ_{ms}, and conclude that the electron momentum, p, and tracking resolution, σ_{track}, are inversely related, i.e.

$$\sigma_{\text{track}} \sim {}^{1}/_{p}. \tag{2}$$

3 Experimental Method

The experimental setup described above allows for two different measurements to be made; the track curvature of the particle trajectory, facilitating a momentum measurement, and a tangential angle along two of the modules, enabling a determination of the angular beam divergence. At the heart of either of these measurements lies the track reconstruction, an example of which is illustrated in the *event display* below (see Fig. 6).

[a] Electrons with an energy of 5 GeV travel at $v = 0.9999998\ c$.

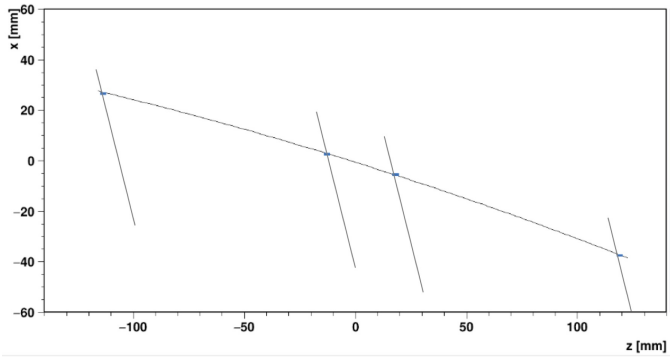

Figure 6: A typical event display (run 2338, $p = 0.8$ GeV/c) showing the four hits along the pixel modules and the reconstructed track (top view). The curvature can be determined from a circle that is fitted to the trajectory. The measurement of the angular divergence is based on a tangent along the central two modules (B and C).

3.1 Curvature Measurement

As mentioned in Sec. 2.2.1, the radius, R, and the curvature, κ, where

$$\kappa = 1/R, \tag{3}$$

can be used to reconstruct the momentum of the incident particle. In the absence of electric fields, a particle of charge q in a magnetic field $\mathbf{B}$ travelling at velocity $\mathbf{v}$, experiences a Lorentz force, $\mathbf{F}_{\mathrm{L}}$, given by

$$\mathbf{F}_{\mathrm{L}} = q\ \mathbf{v} \times \mathbf{B}. \tag{4}$$

The particle of mass m follows a circular orbit and feels a centripetal force, $\mathbf{F}_{\mathrm{C}}$, viz.

$$\mathbf{F}_{\mathrm{C}} = \frac{mv^2}{R}\hat{\mathbf{r}}, \tag{5}$$

where $\hat{\mathbf{r}}$ is a unit vector in the radial direction. The two forces must balance, and, noting that the three vectors are all (roughly) perpendicular to each other, we arrive at an expression for the momentum, namely

$$p = 0.3\ R\ B, \tag{6}$$

where we have adopted conventional particle physics units ($[p] = \mathrm{GeV}/c$, $[q] = e$, $[v] = c$), and taken $c \simeq 3 \times 10^8$ ms^{-1}.

3.1.1 Gaussian Fitting

The curvatures are obtained numerically by fitting to the trajectories circular arcs ([5], [6]). These circular arcs have a well-defined radius, and the inverse thereof is taken to be the curvature. These curvatures are roughly normally distributed, which allows us to employ a Gaussian approximation (barring asymmetric tails from low-p electrons). The mean, μ, of the distribution is the mean curvature, and the width of the Gaussian curve, σ, is the curvature spread. A typical curvature distribution with a Gaussian approximation is shown in Fig. 7.

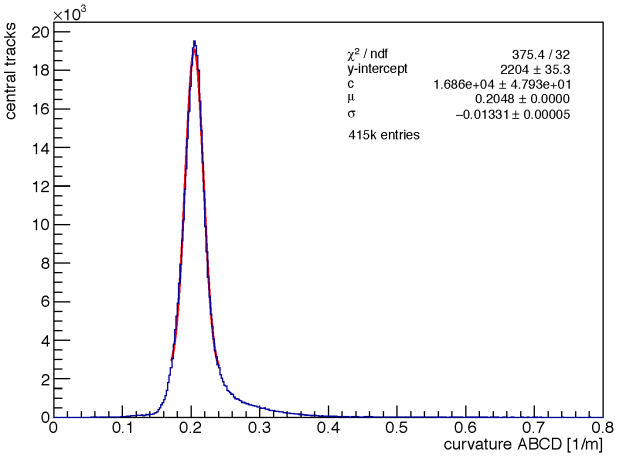

Figure 7: A typical curvature distribution including a Gaussian approximation (red curve). The data shown are from run 2338 at $p = 0.8$ GeV/c. The fits are applied only in the region above $^1/_8$ of the peak in order to ignore asymmetric low-p tails. The mean curvature here is $\mu = 0.2048$ m^{-1} with a spread of $\sigma = 0.0133$ m^{-1}. The relative spread is $^\sigma/_\mu = 6.49\%$. c is a scaling constant.

3.2 Tangential Measurement

The Lorentz force along the y direction (parallel to the magnetic dipole field lines) is zero, which means that their y coordinate is not affected by the field. Any spread of values along this direction is due to the angular divergence of the beam. We measure a tangent in the y direction along modules B and C, called θ_y. The distributions of this variable, to which the same Gaussian fitting procedure is applied, yields the angular spread of the test-beam line.

3.3 Statistical Analysis

Our main goal is to determine the momentum spread; however, the observable studied is the curvature and its spread. If one considers *relative* spreads, i.e. the width of a distribution, σ, as a fraction of its mean, μ, the momentum spread winds up being the same as the curvature spread. This is demonstrated in the following section.

3.3.1 Relative κ Width vs. Relative p Width

Starting from Equations (3) and (6), and taking into account the general formula for uncertainty propagation, we can establish

$$\sigma_p = \sqrt{\left(\frac{\partial p}{\partial \kappa}\right)^2 \sigma_\kappa^2}. \tag{7}$$

Inserting the partial derivative and substituting back the definition of p in terms of κ, we obtain the desired equality, namely

$$\frac{\sigma_p}{p} = \frac{\sigma_\kappa}{\kappa}. \tag{8}$$

We thus note that *relative curvature width* and *momentum spread* describe the same quantity.

3.3.2 Error Propagation

The uncertainty of a measurement along x within the CMS pixel modules, σ_x, depends on both the tracking resolution, $\sigma_{\text{track},x}$, and the beam spread, σ_{beam}. Accordingly, we combine the errors in quadrature, viz.

$$\sigma_x^2 = \sigma_{\text{beam}}^2 + \sigma_{\text{track},x}^2. \tag{9}$$

$\sigma_{\text{track},x}$ is obtained experimentally via a baseline measurement with $B = 0$ T, at $p = 5.2$ GeV/c to minimise effects from multiple scattering. In the absence of a magnetic field in this measurement, there is no Lorentz force along x, leaving the electrons' x coordinate unchanged. We should thus expect a mean curvature of zero along x, and the width of this distribution[b] is taken to be $\sigma_{\text{track},x}$. We remark that $\sigma_{\text{track},x}$ is inversely proportional to the momentum (see Sec. 2.3), and that a series of baseline measurements at all momenta is preferable. $\sigma_{\text{track},x}$ at $p = 5.2$ GeV/c is close to the low-end limit, and thus provides a minimal correction to σ_{x}.

3.3.3 Statistical Variance

Our main measurement parameter herein is the width of the κ distributions, i.e. a function of the variance of the p distributions. In order to assign a standard deviation to the momentum-spread measurements and demonstrate statistical significance, we require further analysis of the measured variance.

As a function of random variables, a sample variance lends itself to statistical analysis. By Cochran's theorem [2], a sample variance, s^2, follows a χ^2 distribution [8, p. 96], from which it can be shown that

$$\sigma(s) = \frac{\sigma_{\text{sample}}}{\sqrt{2N}}, \tag{10}$$

where $\sigma(s)$ is the standard deviation of the width of the sample distribution, N is the sample size (typically large) and σ_{sample} is the standard deviation of the original distribution in question. We thus have the statistical tool needed to assign random errors to the widths of our distributions.

3.3.4 Systematic Uncertainties

The track reconstruction and, consequently, the curvature distributions are highly sensitive to the alignment parameters of the four modules. A potential source of systematic errors in the measurements here presented may stem from a slight misplacement due to the manual fixture of the modules onto the plate. To assign systematic error bands

[b] Note that for consistency the Gaussian fitting procedure here applied is identical to the one for the curvature along x.

to the measurements, we allow for a variation of the module distances A-B and C-D of ± 3 mm, and choose the two distributions that most deviated from the nominal ones out of the four possible. The four systematic variations employed are summarised in Table 1.

Variation no.	Module A [mm]	Module D [mm]
1	-3	+3
2	+3	-3
3	-3	-3
4	+3	+3

Table 1: Summary of the systematic variations considered based on the possibility of misplaced modules. The distances are given relative to the nominal spacing of the modules, i.e. -103 mm ($+103$ mm) for module A (D).

4 Results

The following results are obtained using four CMS upgrade pixel modules in a dipole magnetic field of $B = 1.35$ T, operated at a coil current of $I = 1400$ A. Nearly the entire range of possible momenta is explored, from $p = 0.8$ GeV[c] to $p = 5.6$ GeV, in intervals of $\Delta p = 0.4$ GeV (0.2 GeV in the low-p region from 0.8 to 1.2 GeV), yielding 14 data points overall. Roughly 3-5 million events are triggered per point at a rate of about 5 kHz, and data are collected using the `EUDAQ` framework [9].

4.1 Curvature Method

4.1.1 Momentum Spread

The momentum spread, σ_p/p ($=\sigma_\kappa/\kappa$), as a function of the nominal electron momentum is shown in Fig. 8. The largest momentum spread is observed at $p = 0.8$ GeV (18.63 ± 0.04 (stat) $^{+4.90}_{-4.40}$ (sys)), dropping to 2.02 ± 0.01 (stat) $^{+0.92}_{-0.18}$ (sys) % at $p = 5.6$ GeV. We point out that the track resolution subtracted from the curvature width is an underestimate, as it comes from a high-p measurement. The curve shown is hence a conservative upper limit, as larger resolution corrections can be subtracted at low p given the availability of the according baseline measurements.

4.1.2 Reconstructed Momentum

The measured momentum as determined from the curvature fits as described above, p_{meas}, as a function of the nominal test-beam momentum, p_{beam}, can be seen in Fig. 9. At $p = 0.8$ GeV, p_{meas} lies 10.00 ± 1.13 (stat) $^{+6.25}_{-5.30}$ (sys) % above p_{beam}. At $p = 5.6$ GeV, p_{meas} is 6.43 ± 0.36 (stat) ± 4.82 (sys) % below p_{beam}. The measured momentum agrees with the claimed values within systematic uncertainties.

[c] For convenience, we will from now on drop the factor of $1/c$ when quoting momenta.

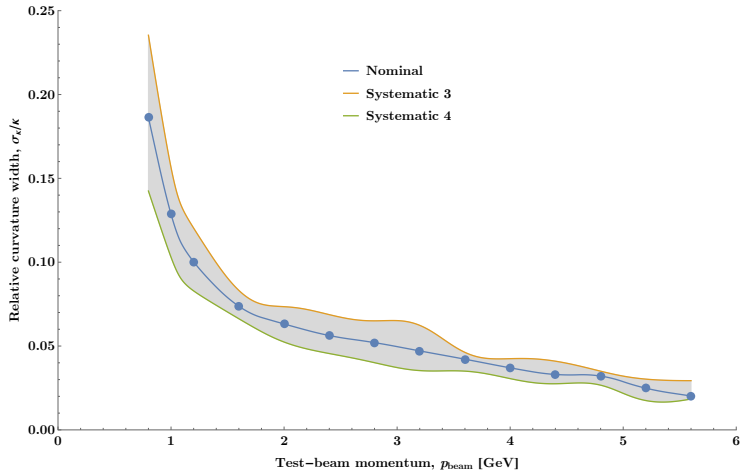

Figure 8: The momentum spread as a function of the nominal beam momentum. The spread drops from an initial $\sim 20\%$ to roughly 3% at high p_{beam}.

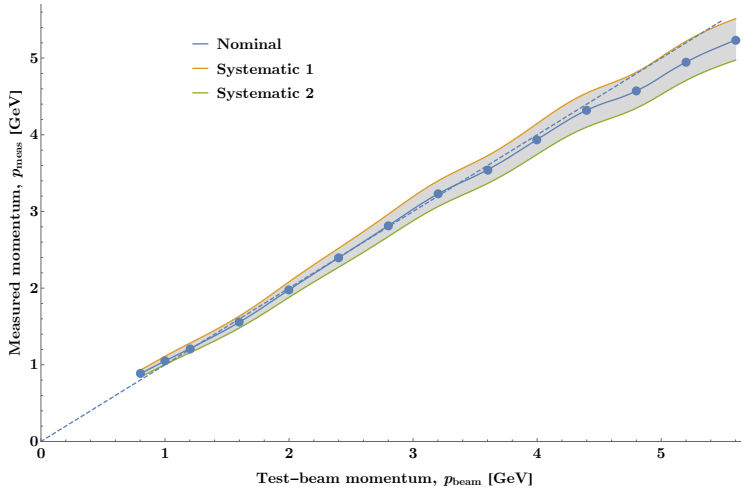

Figure 9: The reconstructed momentum, p_{meas}, plotted against p_{beam}. p_{meas} is consistent with p_{beam} within the error bands shown.

4.2 Angular Beam Divergence

The results obtained using the tangential beam-divergence measurement are depicted in Fig. 10. The curve follows an asymptotic trend, with an initial value of $\sigma_y = 2.59 \pm 0.01$ (stat) $^{+0.11}_{-0.12}$ (sys) mrad at $p = 0.8$ GeV, and $\sigma_y = 0.62 \pm 0.01$ (stat) $^{+0.03}_{-0.02}$ (sys) mrad at $p = 5.6$ GeV.

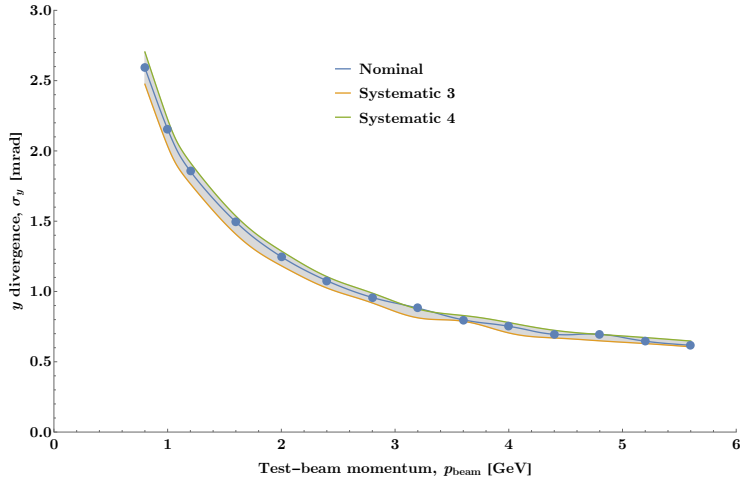

Figure 10: The beam divergence, σ_y, as a function of p_{beam}. Starting at ~ 2.5 mrad at low p, σ_y decreases to ~ 0.6 mrad at higher p.

5 Conclusion

Measurements of the momentum spread and angular divergence at DESY's test-beam line 21 have been presented in this report. Four CMS upgrade pixel modules were placed in a magnetic dipole field of $B = 1.35$ T and used to make measurements of electron trajectories of energies from 0.8 to 5.6 GeV.

Circular fits were applied to the curved electron tracks in the plane perpendicular to the dipole field, whose distributions allowed for the reconstruction of the momenta and their spreads. The momentum spread drops from an initial $\sim 20\%$ at $p = 0.8$ GeV to roughly 3% above $p = 5.2$ GeV. The measurements obtained provide a conservative upper limit, as the error correction due to the track resolution is underestimated at lower p. The reconstructed momentum agrees with the nominal momentum within systematic uncertainties.

Measurements of the particle positions along the dipole-field lines (along y), were performed to obtain the angular beam divergence, which was shown to be ~ 2.5 mrad at $p = 0.8$ GeV, and to drop to ~ 0.6 mrad at the high end of the range of beam momenta considered.

In both measurements, systematic errors were accounted for by introducing a variation of an alignment parameter whose accuracy is constrained due to the manual mounting of two of the modules.

As discussed in Sec. 2.3, multiple scattering causes the track resolution to be a function of the beam momentum. In future experiments, it is recommended to perform baseline measurements in the absence of magnetic fields over the entire momentum range. These would provide more accurate error corrections from the track resolution and could marginally improve the results here presented.

Acknowledgements

I would like to give sincere thanks to my supervisors for their support throughout this project. Thank you, Daniel Pitzl, for your guidance and sharing your insights into many aspects within and beyond this work – be it particle physics, programming, data analysis, hardware, mathematics, or other topics. Thank you, Paul Schütze, for introducing me to the test beam and DESY in general, and for your help on data taking, programming, the operation of the test beam, and this report. Working with and learning from both of you has been a pleasure.

I wish to thank the DESY summer student organising team for running this programme and making this opportunity possible.

References

[1] S Chatrchyan et al. Commissioning and Performance of the CMS Pixel Tracker with Cosmic Ray Muons. *Journal of Instrumentation*, 5, 2010.

[2] William G Cochran. The distribution of quadratic forms in a normal system, with applications to the analysis of covariance. *Mathematical Proceedings of the Cambridge Philosophical Society*, 30:178–191, 1934.

[3] CMS Collaboration. The CMS experiment at the CERN LHC. *Journal of Instrumentation*, 3(08), 2008.

[4] DE Groom and SR Klein. Passage of particles through matter. *The European Physical Journal C-Particles and Fields*, 15(1-4):163–173, 2000.

[5] Veikko Karimäki. Effective circle fitting for particle trajectories. *Nuclear Instruments and Methods in Physics Research Section A: Accelerators, Spectrometers, Detectors and Associated Equipment*, 305(1):187 – 191, 1991.

[6] Veikko Karimäki. Fast code to fit circular arcs. *Computer Physics Communications*, 69(1):133 – 141, 1992.

[7] H Chr Kästli, M Barbero, W Erdmann, Ch Hörmann, R Horisberger, D Kotlinski, and B Meier. Design and performance of the CMS pixel detector readout chip. *Nuclear Instruments and Methods in Physics Research Section A: Accelerators, Spectrometers, Detectors and Associated Equipment*, 565(1):188–194, 2006.

[8] Keith Knight. *Mathematical Statistics*. Texts in Statistical Science. Chapman and Hall, New York, 16 edition, 2000.

[9] Hanno Perrey. Eudaq and eutelescope software frameworks for testbeam data acquisition and analysis. *PoS Proc. Sci.,(TIPP2014)*, 353, 2014.

[10] Paul Schütze. Energy calibration of the DESY test beam in beamline 21, 2013. DESY Summer Student Report. URL: `http://www.desy.de/2011summerstudents/2013/reports/schuetze.pdf.gz`.

[11] Simon Spannagel. *Test Beam Measurements for the Upgrade of the CMS Pixel Detector and Measurement of the Top Quark Mass from Differential Cross Sections*. PhD thesis, U. Hamburg, Dept. Phys., Hamburg, 2016.

[12] DESY Test-beam Coordination Team. Test beams at DESY. Online, 2016. URL: `http://testbeam.desy.de/` [cited August 29, 2016].